

Part III

PROPERTIES OF MATRICES
AND COMPOSITES

STRUCTURE OF PYROCARBONS

X. Bourrat

1 Introduction

Pyrocarbon is the solid form of carbon deposited on a hot surface by cracking of gaseous or liquid hydrocarbons. Pyrocarbon is made up with small or extended graphene layers of sp^2 hybridized carbons more or less saturated with hydrogen. But what makes his a unique character is that these graphene layers can be piled in a high anisotropic way along the deposit surface. The *anisotropy* of the texture and the *density* are the key parameters characterizing this material with also the *size distribution of the layers* and the *hydrogen content*.

Three main events have boosted researches in the second half of the twentieth century: the discovery of carbon/carbon composites at the end of the fifties and their application as strategic material (Lamicq, 1984; Buckley, 1993). Pyrocarbon is the major matrix material. Then pyrocarbons were developed to be used as coating in nuclear fuel industry in the sixties for which the fluidized bed processing was widely developed, that is the chemical vapor deposition (CVD) of high temperature pyrocarbons (Bokros, 1969; Lefevre and Price, 1977). Finally, the strong development of carbon brakes in the last two decades of the twentieth century has focused the interest on infiltration of low temperature pyrocarbon (chemical vapor infiltration, CVI). Many other applications are existing. But the expansion of the carbon/carbon brakes, market the necessity to lower the prices (for fast train and truck markets) and the emergence of new comers has intensified the research all other the world at the turn of the century.

Nowadays the main issue is a fine control of structure with more and more accuracy. The main interest is focused on low temperature pyrocarbon for CVI with the highest deposit rate at lowest price. Local probes are needed to measure the main properties as, e.g. the elastic properties, thermal conductivity and naturally nanostructure parameters, i.e. anisotropy, density, graphene structure or closed porosity, etc.

First, this chapter will rationalize the very different pyrocarbon types following the two major transitions: *low* and *high temperature transitions*. Then in the next part, the recent efforts achieved to relate the structure (and texture) to the processing conditions in the case of low temperature pyrocarbons will be documented: carbon layer, cones and regenerative features. Finally, is a review of the growth mechanisms in relation with structure development and various approaches to quantify the structural parameters: density and anisotropy.

2 The various pyrocarbons

Bokros (1965, 1969) introduced a first comprehensive distinction among pyrocarbons by means of optical microscopy. At that time four structural groups were distinguished

based on their appearance when observed under polarized light (on polished sections). The main concern was the deposition using the fluidized-bed CVD in a broad range of temperature.

Then, Kotlensky *et al.* (1971), Granoff and Pierson (1973), and principally Lieberman and Pierson (1974, 1975) documented the case of carbon composite infiltration at low temperature ($T < 1400^\circ\text{C}$) and low partial pressure of hydrocarbon. They were the first to study the texture in relation with the processing conditions: matrix texture fall into three major types identified as rough laminar (RL), smooth laminar (SL), and isotropic pyrocarbons (I). They were the first to establish the important low temperature transition between rough and smooth laminar for infiltration process.

2.1 The low temperature transition: SL \leftrightarrow RL (800–1,400°C)

Nowadays, the transition between high and low density pyrocarbons is well established. It is under control of the gas phase species, itself controlled by the residence time (Dupel *et al.*, 1995), the temperature or pressure. Transition is due to a change in the heterogeneous growth mechanisms in the range of 800–1,400°C (Féron *et al.*, 1999). These transitions could be called the CVI transitions because it is of major concern in 3D preform infiltration (Lavenac *et al.*, 2000). A progressive passage from SL to a low-density I was also clearly established at very short residence time (and/or lower temperature and pressure) (Lavenac *et al.*, 2001). This passage occurs through the intermediate of dark laminar (DL) (Doux, 1994) by a progressive increase of disclination defects in the hexagonal lattice, the *pentagons* (Bourrat *et al.*, 2001):

SL \leftrightarrow RL

2.1.1 Smooth laminar pyrocarbon (SL)

When observed by reflected light SL is characterized by a medium reflectance (see Fig. 8.1). (Reflectance measures the ratio of light reflected by the polished surface.) Under cross-polars SL exhibits a large and well defined extinction cross known as the “Maltese-cross” (around fiber cross-sections). When rotating the stage, the rolling extinction parallel to the polars is smooth, thus this texture is called “smooth” laminar pyrocarbon. An example of this texture is provided on Fig. 8.1a. When measured, the density is found to be intermediate $1.8 < d < 1.95$. The anisotropy is medium too: extinction angle, A_e , measured in cross-polarized light is $12^\circ < A_e < 18^\circ$ on a scale which goes up to 22 (see Section 5.3). The orientation angle, OA , measured by electron diffraction is $40^\circ < OA < 70^\circ$. OA measures the disorder along the anisotropy plane which decreases down to 15° .

2.1.2 Rough laminar pyrocarbon (RL)

This texture has a high reflectance. When observed with the polarizer alone and because of carbon dichroism, a gray branch parallel to the polarizer appears around fiber cross-sections: reflectance is higher parallel to the graphene planes. Under crossed polars a highly contrasted Maltese-cross appears around the fiber cross sections (Fig. 8.1b). The extinction of the branches is irregular. For that reason it is called “rough” laminar. The roughness is provided by the prismatic texture due to the formation of fine cones generated on fiber

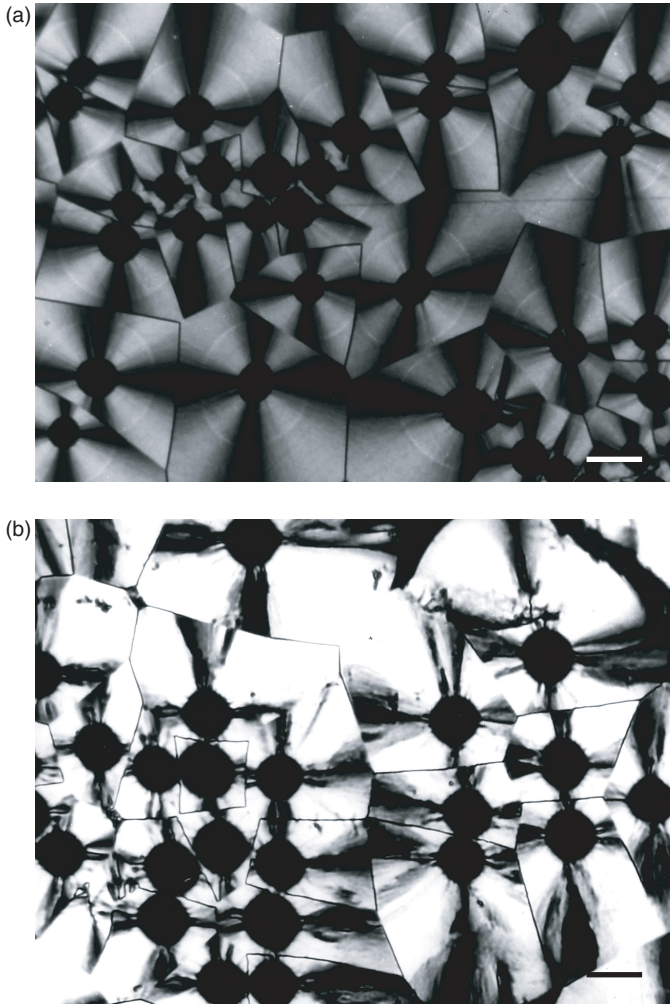


Figure 8.1 Low temperature transition in CVI conditions: (a) SL: smooth laminar pyrocarbon and (b) RL: rough laminar pyrocarbon (Cross-polarized light, bar is $10\ \mu\text{m}$, after Doux, 1994).

surface asperity and transmitted across the whole deposit (see Section 3.2). RL density is high : $2.0 < d < 2.2$. Anisotropy is high too: $A_e > 18^\circ$ up to the maximum (app. 22°) and OA the disorder is low $< 25^\circ$ (typically 15°).

2.1.3 Isotropic pyrocarbon (I)

Isotropic texture has a low reflectance and a very weak anisotropy (or not). Under cross-polars a faint Maltese-cross can hardly be seen. It shows very fine grains with a poor brightness. This texture is often mingled with “isotropic-sooty” pyrocarbons (Section 2.2). The later can have a high density whereas isotropic (ISO) of low density systematically

exhibits a low density: $d \sim 1.6$. The measure of the extinction angle gives values lower than 4° .

2.1.4 Dark laminar pyrocarbon (DL)

Dark laminar has no particular interest, it is only an intermediate in the passage between isotropic and smooth laminar pyrocarbons (SL). As isotropic, it does not seem to be resulting from a different mechanism but the same heterogeneous mechanism as smooth laminar (Bourrat *et al.*, 2001). It is defined by a faint anisotropy and intermediate density: $4^\circ < Ae < 12^\circ$ and $1.6 < d < 1.8$.

2.2 The high temperature transition: $L \leftrightarrow G \leftrightarrow IS$ (1,400–2,000°C)

In the CVD range of 1,400–2,000°C, as processing temperature is increased, density decays and then restores again. This characterizes the high temperature transition reported by many authors in the case of surface deposition (see Fig. 8.2). This second transition towards an “isotropic” grade grown at high temperature was first reported by Brown and Watt (1958). Diefendorf (1970) observed that what is responsible is the “soot” nucleated in gas phase and that it can be avoided by decreasing the hydrocarbon partial pressure (Diefendorf, 1960) as shown in Figs 8.2 (bold line) and 8.3. All these experimental data have been confirmed by many authors in fluidized bed (Bokros, 1965) or static one (Tombrel and Rappeneau, 1965).

Later on, Loll *et al.* (1977) have shown that this transition from laminar (L) to granular (G) and isotropic sooty (IS) pyrocarbon was also existing in the case of CVI (of felt) as shown in Fig. 8.4 under the form of an existence diagram.

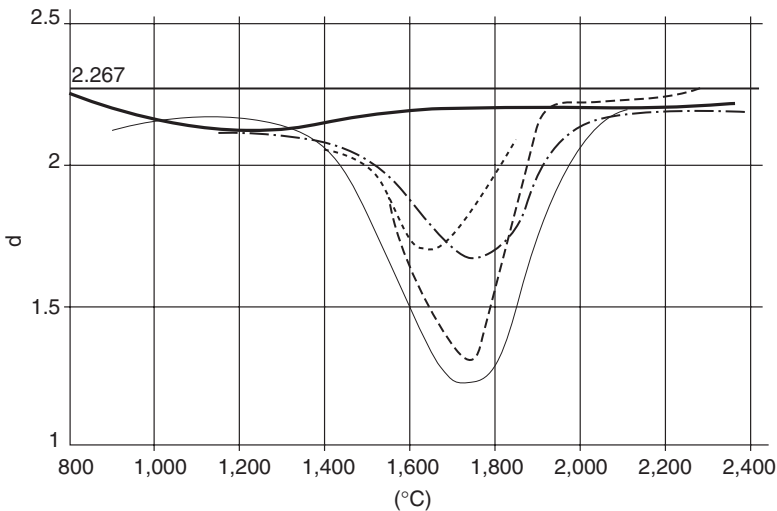


Figure 8.2 High temperature pyrocarbon transition: density versus processing temperature. Full bold line: Diefendorf (1960) 2.3 Pa CH₄; fine dash and dot: *ibid.*, 5.3 kPa CH₄; full fine line: Brown *et al.* (1959) 20 kPa CH₄ or C₄H₄; dashed fine line: Blackman *et al.* (1961) CH₄ and bold dot and dash: Mayasin and Tesner (1961): 100 kPa H₂ and 2 to 10% CH₄.

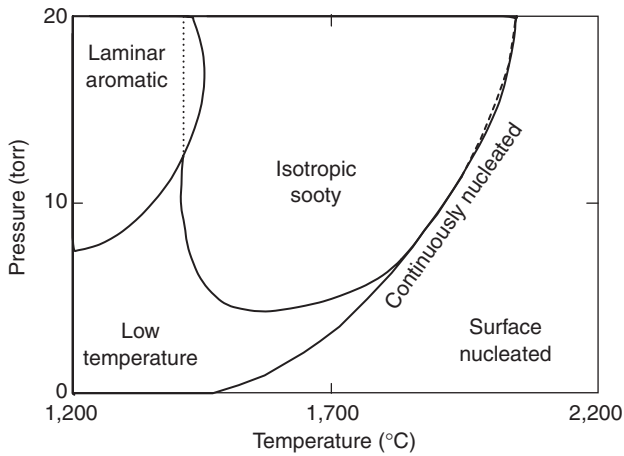


Figure 8.3 High temperature transition after Diefendorf (1970).

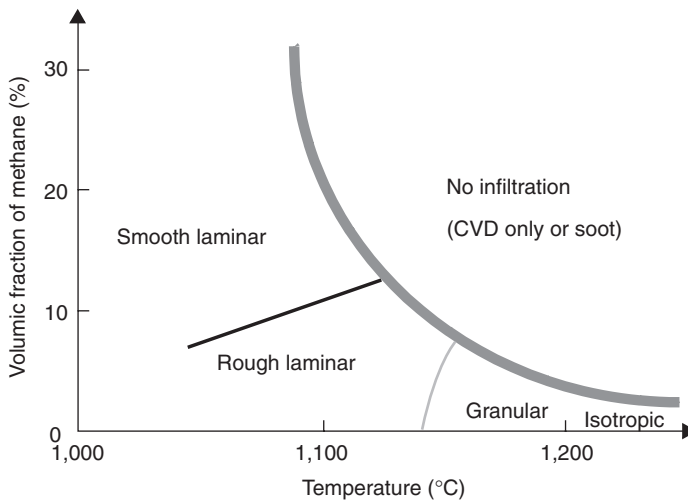


Figure 8.4 Existence diagram of the low temperature transition demonstrated in infiltration of a felt. After Loll *et al.* (1977).

The structural aspects of the growth mechanisms were studied by Kaae *et al.* (1972) and Kaae (1975, 1985). With increasing temperature, laminar pyrocarbon is more and more regenerated by gas-phase nucleated particles as shown in sketch of Fig. 8.5. Transition occurs from regenerated laminar (Fig. 8.6a) to granular (Fig. 8.6b) and to isotropic sooty (Fig. 8.6c, d).

2.2.1 Granular pyrocarbon

It results from a mechanism where most of the carbon still grows directly onto the surface (molecular condensation) but gas phase-grown particles regenerate continuously

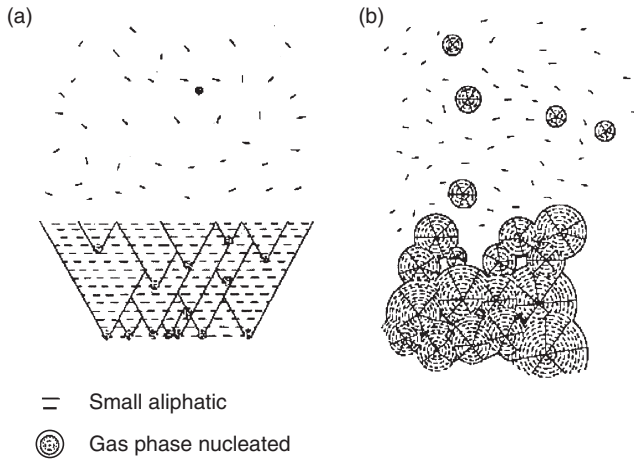


Figure 8.5 Model of the mechanism controlling the high temperature transition: (a) Low depositing rate: regenerated-laminar and granular pyrocarbon; (b) High depositing rate: isotropic sooty (case of high density represented after Kaae, 1985).

small cones (Kaae, 1985). Figure 8.5b gives a sketch to rationalize the mechanism (see Section 3.4).

2.2.2 Isotropic sooty

At higher temperature a sort of “isotropic” deposit is observed (Fig. 8.6c) which was named “isotropic sooty” (IS) by Diefendorf (1970). At the beginning, it has a high density ($\rho = 2.0$). The lack of preferred orientation is provided by the size of the gas phase nucleated particles, these free-floating particles are much larger meanwhile too small to be resolved by optical microscopy: deposits look “isotropic” with optical microscopy. As temperature is increased, density progressively decays down to $\rho = 1.6$ (and even 1.5). Kaae shows that the change in density from high to low, is due to the molecular deposition and not to the particles structure which are still dense in most cases. If the molecular deposition is dense, then the density remains high: $\rho = 2$. If this pyrocarbon is porous, the dense core is surrounded by a tangled structure close to that of glassy carbon: then the density drops down to a minimum ($\rho = 1.6$). At higher temperature the density increases again because the tangled structure becomes coarser and then disappears. It is to note that concentration of hydrocarbon can be increased at a given bed temperature with the same effect. With a too low concentration of precursor this transition was not seen (Fig. 8.2).

Results obtained at General Atomic by Kaae were confirmed at CEA by Pelissier and Lombard (1975). As a matter of fact, the high temperature transition appears as a dramatic drop in density together with the occurrence of an isotropic structure. In this range textures are resulting from a different mechanism for which the particles grown in gas phase have a crucial role. Most of the authors agree with Kaae distinguishing L, G, or IS in-between 1,400 and 2,000 °C:



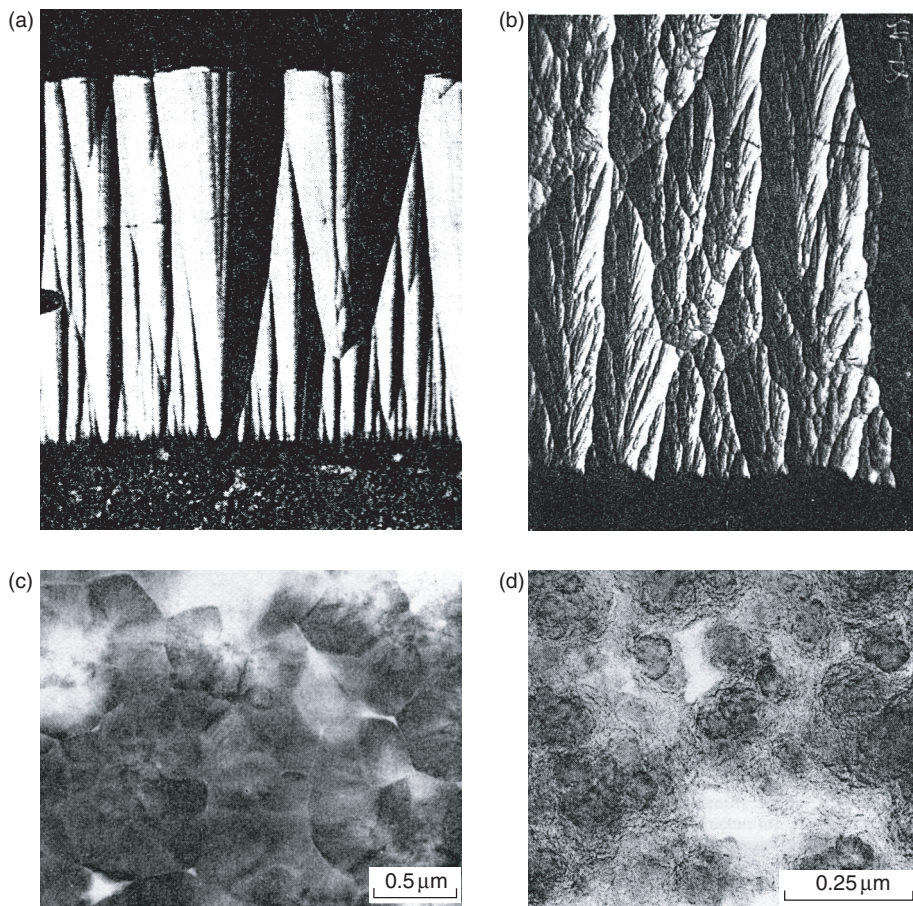


Figure 8.6 Structure evolution during the high temperature transition. (a) Pyrocarbon laminar (few small gas phase-grown particles); (b) Granular pyrocarbon (abundant gas phase-grown particles); (c) IS of high density (abundant dense particles co-deposited with homogeneous pyrocarbon); (d) IS of low density (abundant and dense particles co-deposited with glassy carbon-like pyrocarbon) (a and b: cross-polarized light, bar is 20 μm , after Tombrel and Rappeneau (1965); (c) and (d): TEM after Kaae, 1985).

The high temperature transition has no more been studied till the seventies, in our knowledge.

2.3 Very high temperature pyrocarbons

“Oriented” pyrocarbons used as conductive and gas-tight coating are deposited by CVD of methane at temperatures between 2,000 and 2,500 $^{\circ}\text{C}$ (e.g. 2 kPa of methane at 2,000 $^{\circ}\text{C}$ with a deposition rate of 100 $\mu\text{m H}^{-1}$, Le Carbone Lorraine, 1975). At higher temperature, works performed (Guentert, 1962; Tombrel and Rappeneau, 1965; Hirai and Yajima, 1967; Bokros, 1969; and Goma *et al.*, 1985) have shown by XRD and TEM that the deposit is highly oriented with a regenerated texture (Fig. 8.7c). It was shown by XRD that they grow with

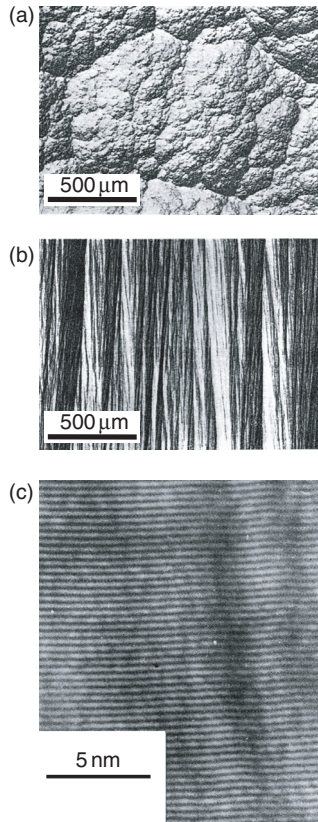


Figure 8.7 Very high temperature pyrocarbon (processing temperature: 2,100 °C): (a) Cross-polarized light on polished surface ($PCH_4 = 0.5$ KPa); (b) Same in cross section (after Tombrel and Rappeneau, 1965); (c) Same pyrocarbon in high resolution TEM (after Goma and Oberlin, 1985).

a turbostratic structure and a high degree of preferred orientation (Guenter, 1962; Tombrel and Rappeneau, 1965). In this case authors speak about direct deposition of carbon with a perfectly oriented turbostratic structure.

2.4 Pyrocarbons issued from new rapid densification processes

The new processes as thermal gradient (Golecki *et al.*, 1995) or pressure-pulse-CVI (Dupel *et al.*, 1994) or film boiling (David *et al.*, 1995; Bruneton *et al.*, 1997), all provide classical textures or combinations of classical features known in CVD, except the possible mixed structures in the case of liquid immersion in the rapid densification process: mosaic pitch-based- and pyrolytic-type carbons (Rovilain, 1999; Beaugrand, 2000) as shown in Fig. 8.8c. It is noteworthy that rough lamellar is much easily produced by I-CVI than by any other process. In most cases, regenerative lamellar (REL) (see Section 3.3) is obtained with the new rapid densification processes.

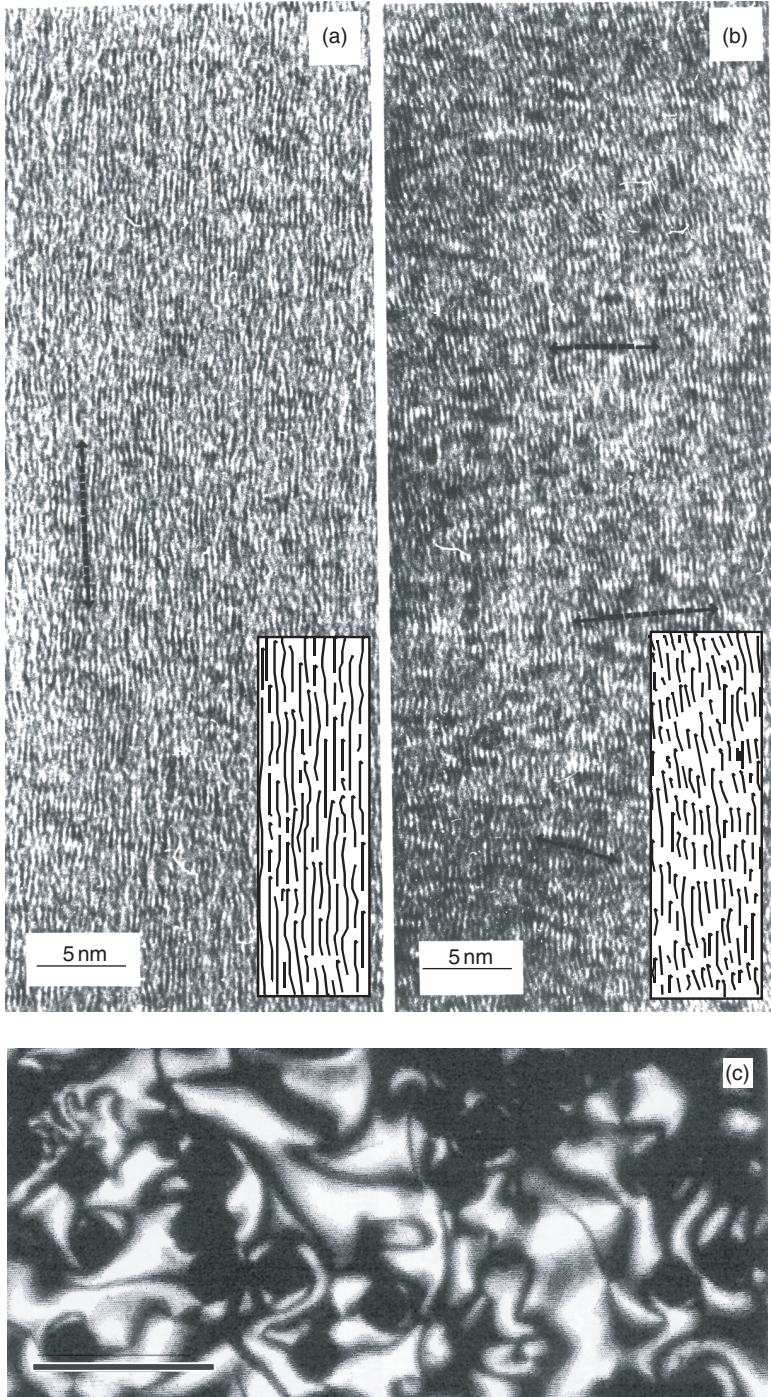


Figure 8.8 New rapid densification processing. (a) Comparison of laminar textures (LRE) obtained by pulse-CVI with a lateral growth of long defective layers with (b) rough laminar pyrocarbon obtained by I-CVI with a good stacking of small and straight layers (Dupel *et al.*, 1995); (c) Mosaic structure that can occur in the film boiling process aside classical laminar textures (after Beaugrand, 2001, bar is 1 μm).

3 Cones and regenerative features

Among the distinctive growth-features of pyrocarbon is the cone generation. These features are important in considering the anisotropy of structure and thermo-mechanical properties, as well as in-service properties (e.g. tribology). Three main mechanisms and their mix have been recognized:

- substrate-generated cones or primary cones;
- secondary cones, self-generated within the deposit;
- secondary cones generated by gas-phase nucleated particles.

Coffin (1964) has modeled the cone formation mechanism. He has definitely shown that they come from a simple roughness transmission effect due to the stacking, layer after layer. It is not the result of a nucleation/growth process.

3.1 Cones formation

Flatness defects which can be transmitted come first from the support roughness. All laminar pyrocarbons possess primary cones generated onto the surface. Rough laminar pyrocarbon alone keeps its primary cones exclusively all across the deposit.

Let us suppose that the surface defect is a sphere lying on the support (Fig. 8.9). Coffin (1964) has shown that the laminar growth propagates the defect layer after layer. At the beginning all asperities at the surface are transmitted exactly with a parabolic shape (2). On both sides of this “paraboloid” surface, the layer direction sharply changes by an angle α as for twinned crystals. This sharp bend when observed on a polished surface perpendicular to the deposit, appears as a parabolic curve with a drastic contrast variation related to the change of the layers direction. This stage lasts more or less depending on surface defects density. Then, the interference of adjacent growing cones leads to a honeycomb structure visible when looking down on the deposit surface. In cross section it shows a prismatic texture (3). The higher the surface roughness, the higher the α angle. This prismatic texture responsible for the rough extinction of the Maltese-cross branches was also called “columnar structure” by Bokros or fibrous structure by Tombrel and Rappeneau (1965) who have extensively studied the generation of cones as a function of temperature during the high temperature transition: laminar–granular transition.

3.2 Surface-generated cones

Rough laminar appears to keep its primary cones across the full deposit. The more probable reason is because rough laminar does develop a highly oriented growth. The superposition of regenerative cones on the primary ones results in the progressive disappearance of them. So the pending question is: why rough laminar does not develop a regenerative growth as all laminars?

Because Rough Laminar pyrocarbon is not regenerative, then primary cones survive providing its prismatic texture. Bourrat *et al.* (2002) have shown that the α angle in-between adjacent columns controls the future “grain boundaries” limiting the lateral graphitization of the crystallites. More importantly they point out that these boundaries control a unique transverse reinforcement in the weakest direction of the matrix (stacking). This is a very important property exclusively known in RL.

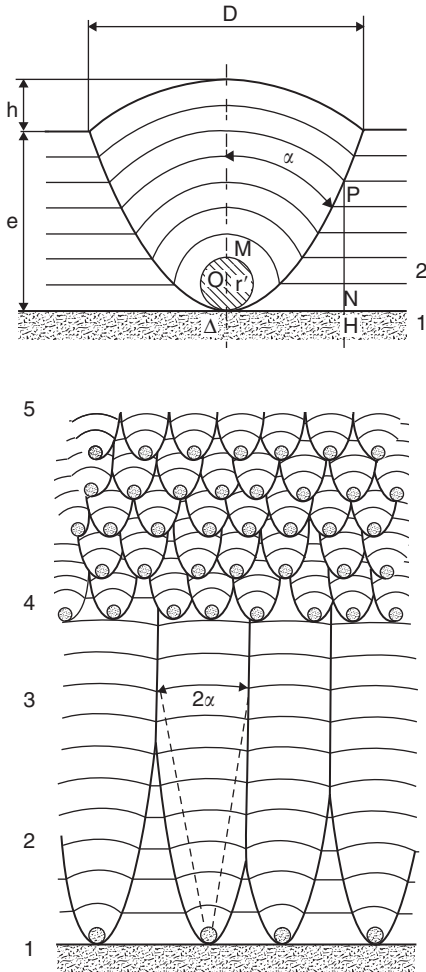


Figure 8.9 Schematic model of cone generation starting from a spherical defect on surface: 1 – surface; 2 – paraboloid zone; 3 – prismatic texture (e.g. RL); 4 – secondary cones as in SL and 6 deposit surface (after Tombrel and Rappeneau, 1965).

3.3 Self-generation of secondary cones

Except rough laminar, all other laminars are regenerative pyrocarbons. Regenerative pyrocarbons appear “smooth.” Regeneration and cones growing mechanism are key features to understand the pyrocarbons, their texture and properties.

3.3.1 Smooth and dark laminar pyrocarbons regeneration

Cones are nucleated within the deposit: *self-generated*. These pyrocarbons develop large layers often convex. Curvatures are related to the presence of pentagons (Fig. 8.10a)

(Bourrat *et al.*, 2001). Thus self-generated growth features, call Ω -like growth features, are formed within the deposit (nanoporosity). They constitute spheroid defects with large radius, r , responsible for the generation of cones as shown in Fig. 8.10b. Because “ r ” is large, the opening of the cone is large, too. The development of a cone stops when a new one generates especially when r is large; for that reason most of the surface-generated cones rapidly disappear (4 in model of Fig. 8.9). Thus, the prismatic columns do not form and the Maltese-cross branches appear “smooth.” This is typically a *self-generation cone mechanism*. This phenomenon is important in controlling the transition:

RL \leftrightarrow SL

As the development of these large cones stops when a new one generate, if the Ω -like features production increases, cones are less and less visible in the passage SL \leftrightarrow DL. At the limit, I is exclusively produced by cone nuclei. As a consequence structure is isotropic, nanoporosity very high and thus density poor.

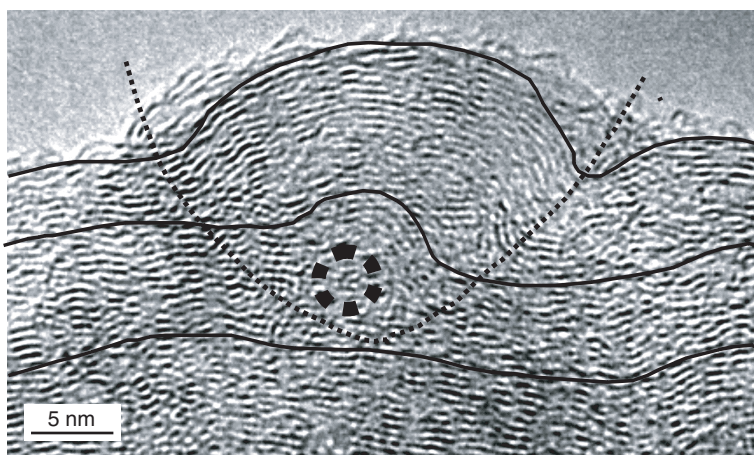
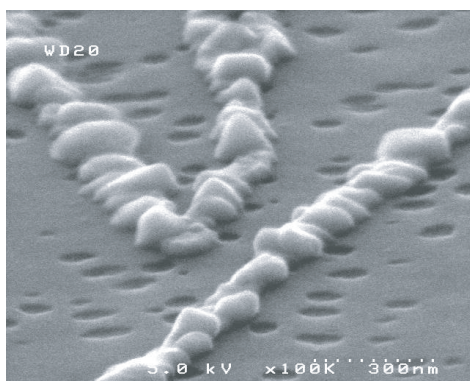


Figure 8.10 Smooth laminar pyrocarbon. (a) Nucleation of curved graphene layers on active sites at the surface of HOPG (Bourrat *et al.*, 2001); (b) Large cones generated by a curved graphene layer (HR-TEM, after Fillion, 2000).

The regeneration of cones produced by the Ω -like growth features gives the smooth aspect to the laminar together with its lower anisotropy and density (Bourrat *et al.*, 2002).

3.3.2 *Regenerative rough laminar pyrocarbons (REL)*

In most of the processes another self-generation of cones occurs, based on a different mechanism. Contrarily to smooth laminar, the cones are generated by small layer defects: α angles measured by TEM darkfield are weak: $15^\circ < \alpha < 18^\circ$ (Fig. 8.11b). The defects in concern lies at nanometric scale, as lattice defects for example. It is assumed that the layer growth mechanism change for a “lateral” mechanism and thereafter the deposit acquires a higher capability to transmit defects. This is referred to as “covering efficiency” of layers (Bourrat *et al.*, 2002).

REL pyrocarbon is formed in different processes that have been alternatively developed: e.g. pulse-CVI (Dupel *et al.*, 1997) or related to the mother molecule, e.g. toluene (Bourrat *et al.*, 2002) or from boron-doped process (Tombrel and Rappeneau, 1965; Jacques *et al.*, 1997). In these processes the layer diameter, L_2 , is systematically larger while the density keeps high. Layers are larger, highly densely packed but paradoxically the coherent lengths are smaller (e.g. pulse-CVI in Fig. 8.8b). It can be assumed that the growth mechanism is mixed: layers grow following the “atom by atom” (or small species) after diffusion onto the surface, with speculative forms as phenyl radical or monocyclic aromatic in the case of toluene. The transition is not precisely known at that time.

3.3.3 *Regenerative features of very high temperature laminar pyrocarbons*

Far from CVI conditions, deposits obtained at very high temperature exhibit the superposition of primary cones and regenerative cones within the deposit (Fig. 8.7b). Thus polished surface of deposit get a fractal appearance known as “cauliflower-like” texture of high temperature pyrocarbon (Fig. 8.7a). The vanishing of previous cones does not occur because the size of the defects are very small and in the same time the hexagonal lattice is perfect and supple enough to transmit any defect at long distance without fading. Goma *et al.* (1985) have shown that layer diameters are indeed very large (Fig. 8.7c). It is probably resulting from a lateral growth mechanism. The covering effect is much higher; the cones are very sharp related to very small defects in the lattice, and transmitted on long distance.

3.4 *Secondary cones generated by gas-phase nucleated particles*

As pointed out very soon by Tesner (1984), blacks and pyrocarbon growth have to be considered as competitive mechanisms but in a given domain of high pressure/temperature. This competition is well documented in the case of granular pyrocarbons for which the nucleation and growth of solid particles in the gas phase is a key step in their growth. These particles by depositing on the growing surface are responsible for the generation of cones (Fig. 8.5a). The different processes, as fluidized bed or static CVD, offer many different combinations. A very wide and open transition occurs, just based on the size of the gas phase particles (improperly called soot), their density and the accessible surface, i.e. surface/volume ratio different on fluidized bed or static surface. All these combinations give rise to the many different granular types reported in the literature.

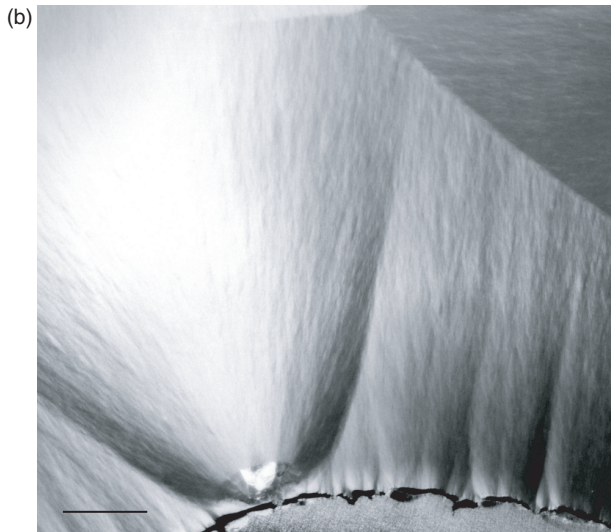
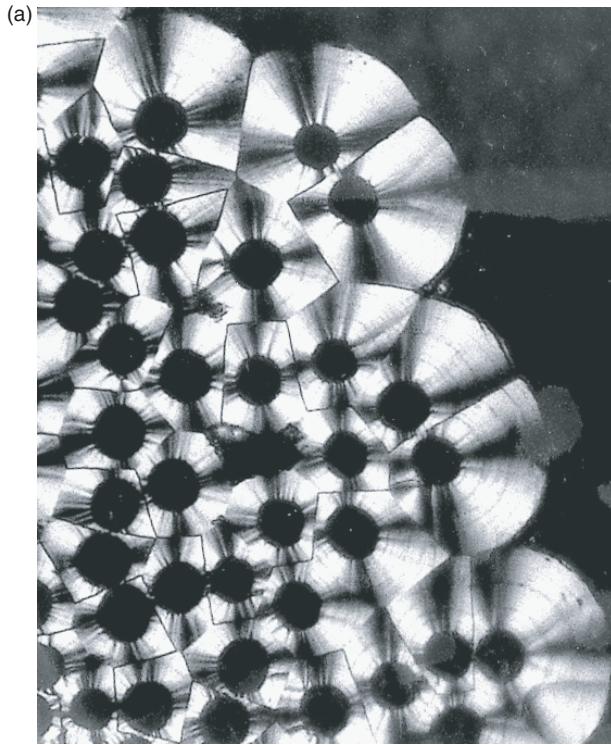


Figure 8.11 Regenerated laminar (P-CVI, toluene 2 kPa, 1,000°C and residence time $t = 2s$) (a) Cross-polarized light: high reflectance and smooth branches of the Maltese-cross, bar is 10 μm ; (b) TEM darkfield: fiber surface-generated cones vanish as secondary cones generate (self-generation); only large cones survive, bar is 1 μm . After Bourrat *et al.* (2002).

4 Carbon layer diameter and growth mechanisms

4.1 Nucleation and heterogeneous mechanisms

The heterogeneous aspect of the pyrocarbon growth mechanism has been very soon the focal point of many experimental and theoretical works. Three different groups of theories have been developed to explain how graphene layers deposit onto the surface. Today the polymorphism of pyrocarbons is clearly related at least to three different heterogeneous mechanisms, controlled by the species present in the gas phase. These species are depending on the mother molecule, the processing pressure, temperature, residence time, and also factors controlling the maturation as diffusion, surface on volume ratio, etc.

- First the Gridale's droplet theory: formulated by Sweitzer and Heller (1956), after Parker and Wolfhard (1950), Stokes (1951), and Gridale (1953), developed by Thomas (1962), and reformulated by several authors. This theory has had a lot of success because of the haze visible in the reactor and attributed to the droplets' diffraction. In fact this haze is more likely the diffraction of solid aerosol particles grown in the gas phase or even HAP molecules. It is admitted, now, that granular pyrocarbons are grown by a mechanism in which solid particles nucleated and partly grown in the gas phase, aggregate in the deposit (Kaae, 1985). This theory is abandoned.
- A second group of theories was based on the direct deposition by a mechanism of chemisorption. The main author of this speculated model is Tesner, then more recently Benzinger and Hüttinger (1999). This mechanism was recently pointed out as one of the main mechanism by Féron *et al.* (1999), Lavenac (2001), Bourrat *et al.* (2001): it takes place in CVI and CVD conditions for the low maturation of the gas phase and probably at very high temperature.
- Finally, authors who postulate that two mechanisms are competitively involved as Diefendorf (1960) or Féron *et al.* (1998) were in the right direction. At low temperature in CVI conditions, the direct deposition of small species by chemisorption on layer edge sites and the molecular condensation of HAP molecules is the best model to match with the transition from smooth to highly anisotropic laminar (Féron *et al.*, 1998). At higher temperature the competition with homogeneous nucleation and growth as speculated by Tessner was also verified by TEM works (Pellissier and Lombard, 1975; Kaae, 1985).

As a summary, according to structural works published in the open literature, three main mechanisms can be considered, based on graphene layer sizes distribution L_2 and the anisotropy of their distribution. Kaae (1985) was more interested by the high temperature transition whereas Bourrat *et al.* (2001) recently documented the low temperature transition. In the following only the two mechanisms related to the low temperature transition will be reviewed.

4.2 Mechanisms controlling the low temperature transition (I-CVD processing)

To evidence this double mechanism, Bourrat *et al.* (2001), have achieved the deposit directly on a TEM carbon grid. All the processing parameters are kept constant except "*t*" the residence time in the hot zone. When "*t*" is very short, dark laminar pyrocarbon is obtained. High resolution TEM shows that the growth occurs out of line in all directions (Fig. 8.12a).

In that case thinning is not necessary; sample is seen “as received.” Layers are extended. The mean fringes lengths L_2 was seen to be high: $\langle L_2 \rangle = 5.8$ nm with a maximal length of 20 nm. Such large layers are resulting from a direct deposition mechanism of small species. Because the residence time is very short, it is concluded that smooth laminar pyrocarbon grows from small species. Indeed, mainly small aliphatic are analyzed by in-situ Infra Red for that residence time (Féron *et al.*, 1999). If the smooth laminar pyrocarbon is deposited on a cleaved surface of HOPG (pyrographite), the deposit occurs only on substrate sites: (00.2) growth steps and grain boundaries as shown in Fig. 8.12 and sketch of Fig. 8.13a. In absence of active sites the growth of smooth laminar does not occur (Bouchard *et al.*, 1999; as seen by STM, Lavenac *et al.*, 2001). So it is concluded that heterogeneous reactions comprising a chemisorption and a dehydrogenation step on active sites are required. Last point is that this mechanism gives rise to large layers with a very low hydrogen content (about 1.5 atomic %) and many curvatures in the layers, induced by the presence of pentagons entrapped in the lattice. Growth of the hexagonal lattice with pentagons disturb the anisotropy and increases the nanoporosity: $d < 2$ (Bourrat *et al.*, 2001).

On the other side, when the residence time of the gas phase is long before reaching the substrate ($t = 4$ s in Fig. 8.12e) the carbon deposit on the carbon grid is different. The mechanism has changed completely due to the maturation of the gas phase. In those conditions highly oriented rough laminar pyrocarbon is deposited. Layers are short, flat and deposited parallel to the anisotropy plane. Fringes length are three times shorter in average: $\langle L_2 \rangle = 1.7$ nm. More importantly, there is no layer larger than 5 nm and no curvature. The deposit is also characterized by a higher stacking coherence L_c . When HOPG is used as a substrate, the whole surface is rapidly and uniformly covered by a flat coating. There is no need for a reaction on any substrate active site to grow the first layers of RL on the substrate (Bouchard *et al.*, 2001). It is deduced from this key experience that the deposit occurs mainly by a step of physisorption of conjugated aromatic polycyclic species (PAH) directly on the surface (Fig. 8.13b). Layer growth still occurs at the edge but mainly by diffusion of large neighboring species. Such a growth mechanism results in a residual hydrogen content higher than that of smooth laminar pyrocarbon (about 3.5 atomic %). Dehydrogenation step is not a critical step in the carbon deposit.

As soon as species are produced with the ability to condense on the surface this mechanism with a higher depositing rate dominates on lateral growth (still active but kinetically much slower). The only control on this sharp transition from one mechanism to the other is the presence in the gas phase of PAH and their capability to condense on the surface with sufficiently high rate to block the chemisorption sites (and lateral growth) on the underlying layers (Bourrat *et al.*, 2001): this is the transition from smooth to regenerative laminar.

5 Density and anisotropy of pyrocarbons

5.1 Pyrocarbon density

Density is a key specification for pyrocarbon. The reason is the very high sensitivity of density to the structure. During the high temperature transition, e.g. a large variation of density can occur depending on processing conditions, i.e. temperature, partial pressure and residence time of the hydrocarbon source. Density is resulting from the growth mechanism controlled by these major processing conditions. But different densities have first to be distinguished.

The *apparent density* is that of the material: mass/geometrical volume.

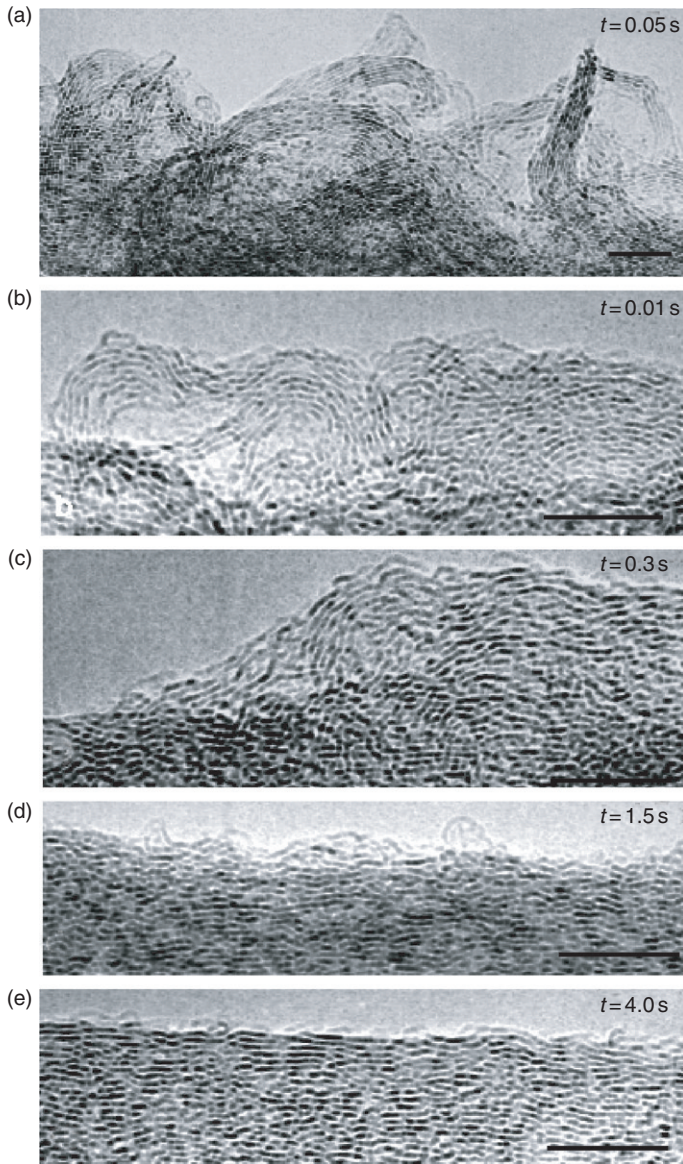


Figure 8.12 Low temperature transition. High resolution TEM micrographs of the growing carbon layers as a function of gas phase residence time “ t ” from dark laminar (a) to smooth laminar pyrocarbon (b)–(d) to highly oriented laminar (e). Bar is 10 nm. After Bourrat *et al.* (2001).

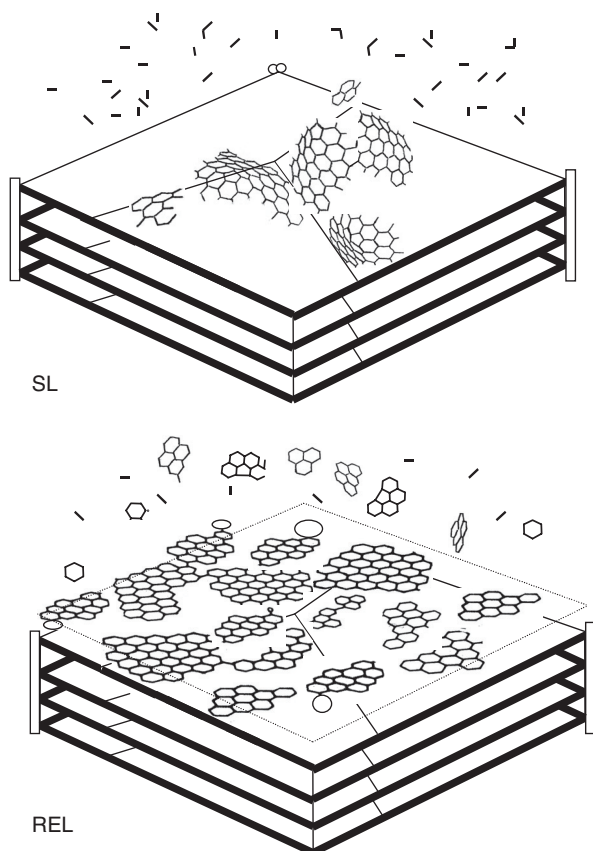


Figure 8.13 Deposition model diagram of smooth (SL) and rough laminar pyrocarbon (REL) on highly oriented pyrographite (HOPG). SL: chemisorption of small species on growing layer edges, dehydrogenation/reaction (according to Bourrat, 2000). REL: molecular condensation on surface and reaction by an edge to edge mechanism.

The *crystallographic density* can be drawn from the lattice parameters: $a = cte = 245.6$ pm and d_{002} -spacing increases as follows:

- graphite value: $d_{002} = 335.4$ pm $d_{cry} = 2.267$
- heat-treated dense pyrocarbon: $d_{002} = 342$ pm $d_{cry} = 2.23$
- as-processed dense pyrocarbon: $d_{002} = 344$ pm $d_{cry} = 2.21$

This calculation does not take into account hydrogen and boundaries in-between the carbon graphene piles in the as-processed pyrocarbon. Anyway, the very high values obtained following this calculation readily show that the paracrystalline structure of pyrocarbon is not easily modeled.

The *helium density* based on the displacement of this very small molecule (helium pycnometry) is a very popular technique. Helium density is often considered as the experimental approach of the crystallographic density: nanoporosity is non accessible by helium. Thus

it is used as a specification to characterize the various textures. In the case of CVI textures rough laminar with the highest anisotropy is measured: $2.0 < d < 2.2$ (as-processed). Smooth laminar has a much lower density: $1.8 < d < 2.0$. Then isotropic textures exhibit values as low as 1.6. The methanol or butanol displacement density is used as a standard in Japan (R 7212).

Water density is a very convenient technique for large pieces. It is also known as the triple weighing technique. (i) First the composite is weighed dry, the mass M_0 is obtained; (ii) an Archimede weighing is then performed in the water providing M_1 ; and (iii) a third weighing of the sample just out of water (no more pouring water) gives M_2 . It can be drawn from these three values the so-called water density, d , and the open porosity, V_p , of the pyrocarbon as follows:

$$d = M_0 / (M_0 - M_1)$$

$$V_p = (M_2 - M_0) / (M_2 + M_1)$$

Also are used techniques as *sink-float density*. Such techniques involve a mixture of dense liquors as bromoform and methanol (Lieberman and Pierson, 1974). Density is determined by suspending ground sample in the density gradient columns.

5.2 Anisotropy as measured by X-ray diffraction

The very high preferred orientation of pyrocarbon is the attractive feature of this form of carbon. The quantification of the anisotropy was recently discussed (Bourrat *et al.*, 2000). Graphene layers tend to align parallel to the surface deposition. Pyrocarbons grow with the hexagonal form of carbon. Unlike graphite, its structure is limited to two dimensions, i.e. the hexagonal lattice of the aromatic layer (graphene). The layers are stacked one on the other with a rotational disorder (no 3D-graphitic order: turbostratic structure (Warren, 1941)). In this stacking, a chance parallel layer occurs giving rise to a local coherent scattering even if not perfectly parallel. The diffracted spots observed in the reciprocal space are not the 001 graphite spots, but the so-called 00l turbostratic interlayer interference (strongest peak: 002). Coherent lengths parallel and perpendicular to the basal plane (L_a and L_c , respectively) are more or less extended, depending on the perfection of the layers.

The different pyrocarbons can be characterized by the size distribution of the carbon layers “ L_2 ” (as defined in the schematic of Fig. 8.14) and the anisotropy of the texture. When they are highly anisotropic, all the layers are parallel to the anisotropy plane. As the anisotropy decreases, more and more layers are misaligned with respect to the anisotropy plane. In the reciprocal space, this gives rise to the polar distribution of the 002 spots. A schematic representation of the preferred orientation is represented in Fig. 8.15 following Pappis and Blum (1961): this is a pole figure. The specimen, e.g. a film of pyrocarbon deposited on a flat surface, is placed in the center of a sphere and the orientation of each coherent domain is indicated by a normal to its basal planes. Wherever this normal penetrates the top surface of the sphere a point is marked. In a case of pyrocarbon, the points gather with a density maximum around the point marking the deposit plane. A continuous decrease is observed as the equator region is approached. Pyrocarbon can thus be described exactly as a polycrystalline material which exhibits preferred orientation.

The easiest experimental conditions require a thick pyrocarbon deposit and a transmission setup. As proposed by Guentert (1962), Tombrel and Rappeneau (1965), or Hirai and Yajima (1967), a small cylinder is drilled across the deposit with its axis parallel to the deposit plane

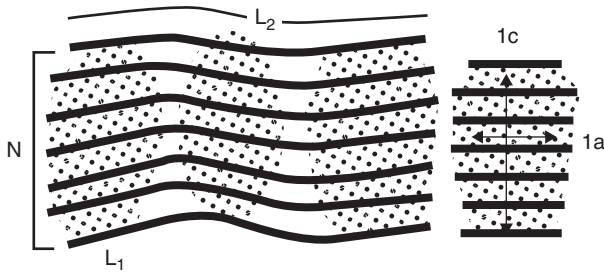


Figure 8.14 Model of turbostratic piles of carbon layers (according to Bourrat *et al.*, 2000).

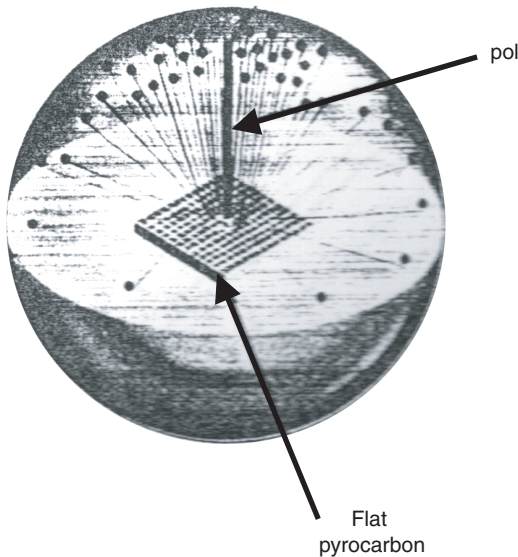


Figure 8.15 Pole figure of pyrocarbon film deposited on a flat support (after Pappis and Blum, 1961).

as shown in Fig. 8.16. Few tenth of millimeters in diameter. This small cylinder is placed on the specimen holder at the center of a regular diffractometer. It is mobile above the θ - 2θ axis of the diffractometer with an angle referred to ϕ . At the starting point, ϕ is adjusted in order to place the anisotropy plane approximately in the plane of the tube and detector. A first step consists to fix θ and 2θ positions (tube and detector, respectively), for the maximum intensity of the 002 peak (around 2θ B 25–26° for a Cu anticathode). Then the intensity $I(\phi)$ is recorded step by step for the different ϕ angles of the sample on its axis. ϕ is equal to 0° for the maximum of intensity. The result is a bell-like curve as represented on Fig. 8.17. Tombrel and Rappeneau compare four different pyrocarbons with lower and lower preferred orientation as the HWHH increases. All the processing computers contain different fitting functions to get the accurate parameter needed to compare the different pole distributions.

When the thickness of the deposit does not allow the sampling of a cylinder, a Euler attachment is required to record the pole figure directly from the flat film. In this case an extra rotation mobility of sample known as the polar χ angle, allows the sample to rotate

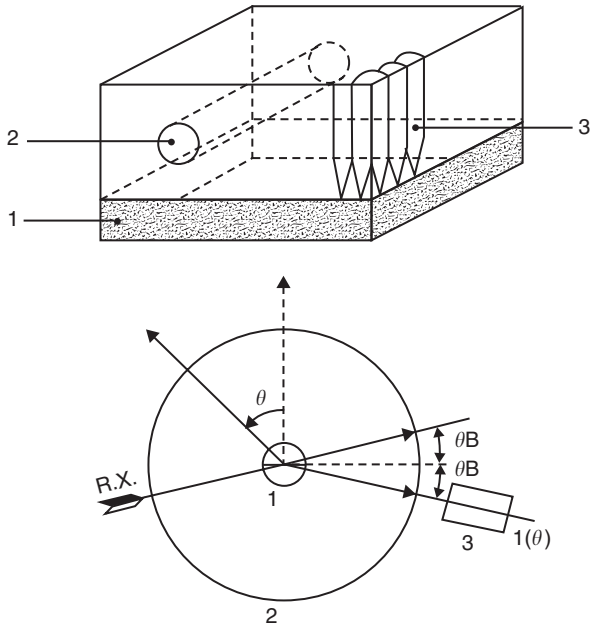


Figure 8.16 Experimental set up in the case of thick deposit and transmission XRD device (after Tombrel and Rappeneau, 1965).

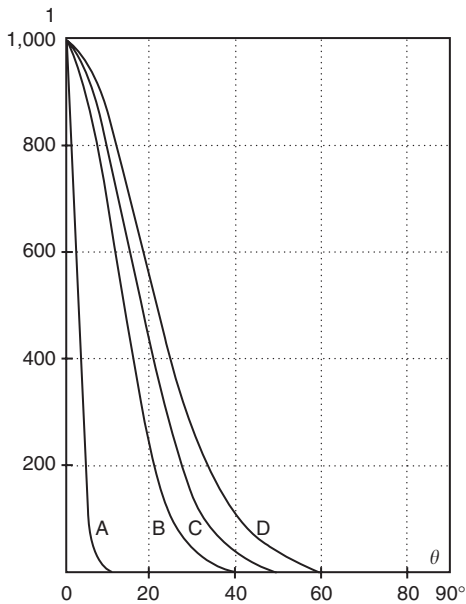


Figure 8.17 XRD anisotropy curves normalized for: A: Regular 2,100 °C pyrocarbon with 0.5 KPa of methane, annealed under compression (0.5 GPa) 1 h at 2,800 °C ($\Delta\theta = \pm 6^\circ$); B: Boron-doped pyrocarbon (0.8%) deposited at 2,100 °C ($\Delta\theta = \pm 13^\circ$); C: Regular pyrocarbon deposited at 2,100 °C with 0.5 KPa of methane ($\Delta\theta = \pm 16^\circ$); D: Super Temp Corp. sample deposited at 2,100 °C from 0.5 KPa of methane ($\Delta\theta = \pm 23^\circ$) (after Tombrel and Rappeneau, 1965).

above the eucentric point as represented in Fig. 8.18. This case is a reflection setup known as the Schulz setup which allow to record pole figure up to $\chi < 65^\circ$ without too much aberrations. This technique allows a direct recording of the pole figure in reflection mode.

5.3 Optical anisotropy (*Ae*)

This optical method is based on the measurement of the apparent reflectance ratio of the pyrocarbon (Bourrat *et al.*, 2000). (The best way is to use a photo-multiplier (PM) (Rouzaud and Oberlin, 1983).) When it is not possible method involves the rotation of the analyzer of a polarization device. It has the advantage to be easily performed. Meanwhile, it requires a deposit at least 2 μm -thick and an optical polishing of high quality. This measurement is only semi-quantitative but it enables to separate the different pyrocarbons of a same family on the basis of anisotropy.

This measure is obtained on polished sections perpendicular to the deposit plane. The simplest technique requires a reflected-light microscope equipped for polarization with a rotative analyzer. An example of the measurement is provided on Fig. 8.19. A fiber with a thick coating is selected. Under cross-polars a Maltese-cross can be observed. When the analyzer is rotated (special attachment) the branches of the Maltese-cross fuse together on the bisector (arrow in Fig. 8.19). The first quadrant gets completely dark and then becomes bright again. At the position of complete darkness the extinction angle “*Ae*” can be read directly on the vernier micrometer of the analyzer. *Ae* is giving a good approximation of the reflectance anisotropy ratio R_o/R_e , by the relation $R_o/R_e = \text{tg}^2(45 + Ae)$. The intrinsic value are probably not exactly that of graphite: different electronic structure, heteroelement as H abundance, etc. Also because of the subjective assessment of compensation and discrepancies between polarizers it is best to consider the *Ae* value directly: the scale generally ranges from $0^\circ < Ae < 4^\circ$ for I, $12^\circ < Ae < 18^\circ$ for SL and $Ae > 18^\circ$ for rough and regenerated laminar pyrocarbons. The highest values obtained are in the range of 22° – 24° (depending on the microscope).

5.4 Optical retardation method

A second optical approach can be derived from the classical measurement of birefringence in the field of mineralogy. The cross section (highest birefringence) is observed under cross polars. Because of the strong birefringence of carbon the two reflected beams impinging the analyzer (ordinary and extraordinary beam) produce an interference color. This color is a grey yellowish of the first order. For reflection, retardation has not the same origin as in transmission: phase shift is low while the interference colors indicate higher values (by using the two-beam approximation given by Michel Levy chart). It can be assumed that the anisotropy is responsible of these color changes. The experimental retardation values that can be measured by different means are effectively changing with the anisotropy: RL is observed with more than 250 nm whereas SL gives values about 150–180 nm and DL is much less (isotope is 50–80 nm). This technique is still under development.

5.5 Anisotropy as measured by electron diffraction (*OA*)

The electron diffraction technique is irreplaceable to analyze pyrocarbon infiltrated in preforms or very thin coatings. Coupled to an image analysis software, it gives the following structure parameters: (i) the orientation angle, *OA*, of the scattering domains which is a measurement of the “geometric” anisotropy; (ii) the interlayer spacing d_{002} which is a basic measurement of the

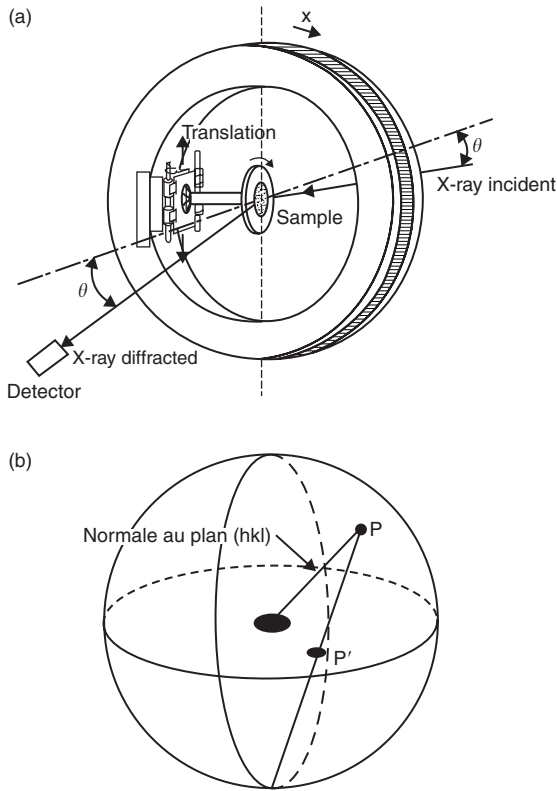


Figure 8.18 Schulz setup for an XRD Euler attachment: (a) for recording the pole figure on thin film (flat support). The pole figure is obtained following the projection shown in (b).

short distance ordering of the carbon turbostratic structure. Other pieces of information can be extracted from the diffraction pattern; (iii) L_c , the turbostratic pile thickness; (iv) L_a the coherent extent of the carbon layer; or (v) P_1 the ratio of graphite stacking in the turbostratic pile.

Orientation angle is determined by selected area diffraction (SAD). The measurement of the azimuth opening of the 002 arcs along the Debye–Scherrer ring is proposed as the OA. The volume which can be analyzed this way is as low as the selected area used to perform the diffraction pattern (100 nm in diameter and few hundred nms thick). The counterpart is the difficulty to get the sample thinned to electron transparency. First the software scan the intensity across the diagram (Fig. 8.20b) passing through the center. The center of the diagram is previously found automatically, provided that the central spot is systematically saturated by the previous intensity correction operated on the image. The program finds out the two 002 maxima, so the “Debye–Scherrer” ring can be drawn, superimposed on the pattern. If the operator agrees with the result, then the intensity is extracted versus the azimuth angle (Fig. 8.20c). The program fits these peaks to two Gaussian curves and the anisotropy OA is given as the mean value of the two widths at half height. The mean full-width at half-height is call “OA” the orientation angle. Physically, it represents the miss-orientation, the disorder of layers along the anisotropy plane (see Bourrat *et al.*, 2000 for more details).

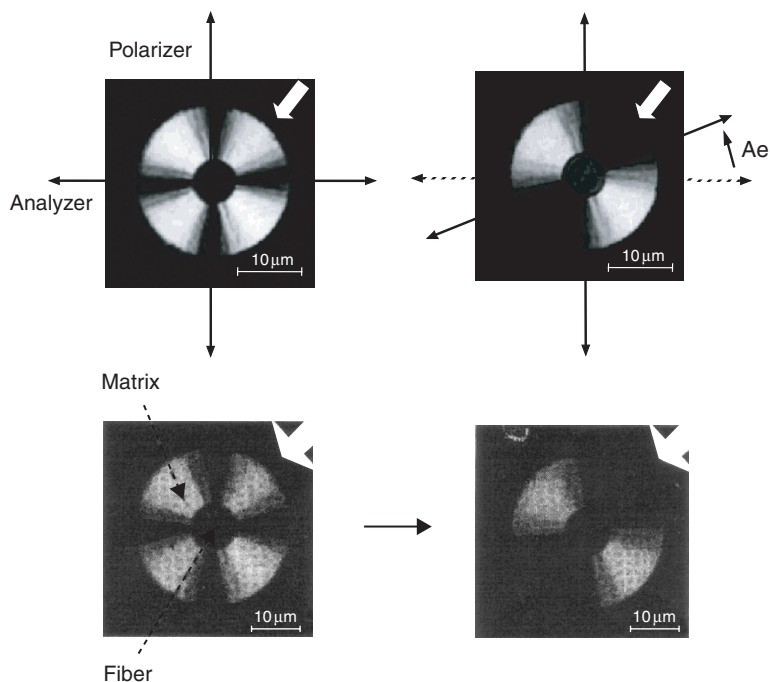


Figure 8.19 Measurement of the extinction angle, A_e , in a pyrocarbon matrix with reflected polarized light (example of a coated fibre) (after Bourrat *et al.*, 2000).

There exists a linear relationship between OA and A_e for most of the lamellar pyrocarbons analyzed by these two techniques as shown in Fig. 8.21. The value of the interlayer spacing (d_{002}) can be obtained as well, after a previous standardization with a graphite pattern, in similar conditions (Fig. 8.20d). Thinning the sample relaxes the internal stress and thus artifacts are numerous with this d_{002} value.

6 Conclusions

- Structural characterization of the pyrocarbon deposit is an essential requirement before discussing all other data as kinetics, or growth mechanisms or even properties. An abundant literature exists which presents no interest because the pyrocarbon structure was not previously defined: the two main properties are *density* and *anisotropy*.
- Survey of structural studies of pyrocarbons, whatever the process and among the whole range of temperature (800–2,500 °C) show that the different growth mechanisms are not so numerous, even if many different microstructures are existing.
- These few mechanisms are controlled by the concentration in gas phase of key species. For that reason, residence time “ t ” and more generally the so-called maturation of the gas phase is an important parameter. As far as we know, the key species are: small radicals, PAH molecules and solid particles nucleated (and grown) in the gas phase.

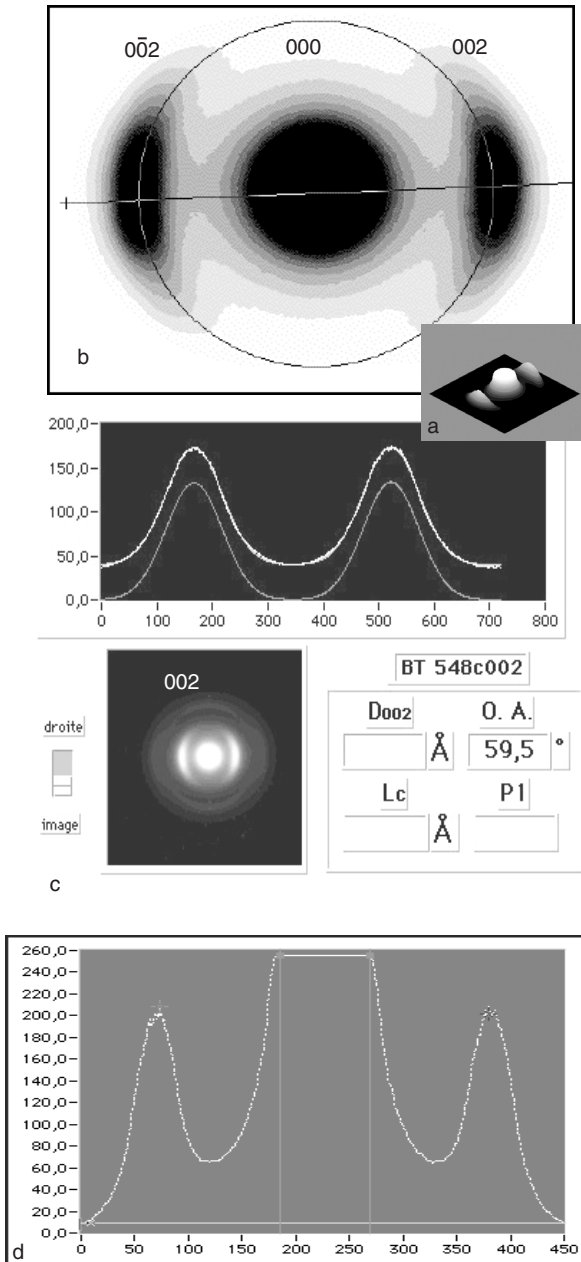


Figure 8.20 Electron diffraction: OA measurement. (a) Experimental pattern; (b) processing of the image analysis; (c) Azimuth plot (white) to be analyzed and Gaussian fit (down) of the experimental intensity. OA is the mean width at half height of the two Gaussian curves; (d) the optional measure of the d_{002} -spacing (after Bourrat *et al.*, 2000).

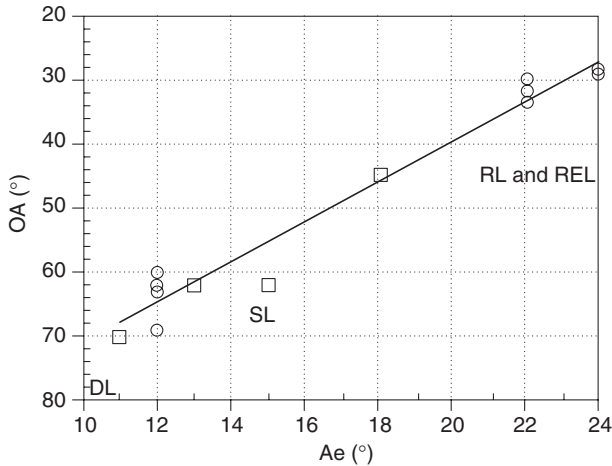


Figure 8.21 Plot of Ae (optical technique) versus OA (electron diffraction technique) (squares after Bourrat *et al.*, 2000; open circles after Féron, 1998).

- At low temperature for the isobaric/isothermal CVI processing of aliphatic hydrocarbons (800–1,400 °C) a competition between two mechanisms controls the transition between the two main textures developed for carbon/carbon composites: (i) the direct growth from small species (lateral growth mechanism); or (ii) the molecular condensation and reaction of PAH. If gas phase maturation is poor, pyrocarbon is a smooth laminar or progressively dark laminar (and finally isotropic). Anisotropy is progressively lost because the over-growth of layers (lateral growth mechanism) concentrates pentagons (buckling of layers). On contrary; if the gas phase maturation is higher, then laminar pyrocarbons can develop as small hydrogenated flat graphene layers (REL):



Gas phase depletion for very high “*t*,” leads to the smooth laminar again in the case where the surface/volume ratio is high for a given residence time.

- At high temperature in the CVD domain (1,400–2,000 °C) the competition occurs between particle growth in the gas phase and direct deposition. This range is still in use by means of fluidized-bed for pyrocarbon (medical biomaterials). If temperature and/or saturation is high enough, maturation is prompt and gas-phase nucleation of particles occurs. Competition arises between the direct deposition of solid particles and PAH: a regeneration of cones is produced by particles with the granular structure. In both processes, fluidized-bed and static CVD, a strong drop in density is observed as the amount of particles increases. In fluidized-bed the structure turns to sooty-isotropic. This transition is existing in CVI (Loll *et al.*, 1977). The low density is related to the development of a fine porosity of the pyrocarbon directly deposited in competition with the particles (Kaae, 1985). This sooty-I is still gas-tight but not graphitizable.
- At very high temperature (2,000–2,500 °C) a laminar pyrocarbon characterized by extended layers is observed with a regenerative texture. This is probably a self-regeneration related to the very high anisotropy and high density.

References

- Bacon, G. E. (1956). *J. Appl. Chem.*, **6**, 477–481.
- Blackman, L. C. F., Saunders, G., and Ubbelohde, A. R. (1961). *Proc. Royal Soc. G.B.*, **264A**, 1316, 19–40.
- Beaugrand, S. (2000). “Etude du procédé de densification rapide par caléfaction pour l’élaboration de composites carbone/carbone,” Univ. Orléans (France).
- Bokros, J. C. (1965). “Variation in crystallinity of carbons deposited in a fluidized bed,” *Carbon*, **3**, 201–211.
- Bokros, J. C. (1969). “Deposition, structure and properties of pyrolytic carbon,” in *Chemistry and Physics of Carbon*, Vol. 5, p. 1, P. L. Walker, Jr ed., Marcel Dekker New York.
- Bomar, E. S., Gray, R. J., and Eatherly, W. P. (19xx) “A technique for measuring preferred orientation in pyrolytic carbon coating using plane-polarized light,” Oak Ridge Nat. Lab. internal Report, 885.
- Bourrat, X. (2000). “Structure of carbon and carbon artefacts,” in *Sciences of Carbon Materials* H. Marsh and F. Rodriguez-Reinoso, eds, ch. 1, Univ. Alicante Publisher.
- Bourrat, X., Trouvat, B., Limousin, G., Vignoles, G. L., and Doux, F. (2000). *J. Mater. Res.*, **15**, 92–101.
- Bourrat, X., Lavenac, J., Langlais, F., and Naslain, R. (2001). “The role of pentagons in the structure of laminar pyrocarbons,” *Carbon*, **39**, 2376–2380.
- Bourrat, X., Fillion, A., Naslain, R., Chollon, G., and Brendle, H. (2002). “Regenerative laminar hydrocarbon,” *Carbon*, **40**, 2931–2945.
- Brown, A. R. G., Clark, D., and Eastabrock, J. N. (1959). *J. Less Common Metals*, **1**, 94.
- Brown, H. R. G. and Watt, W. (1957). Conf. on Industrial Carbon and Graphite, London September 24–26, 1957, Soc. of Chemical Industry, publisher (1958), 86–100.
- Bruneton, E., Narcy, B., and Oberlin, A. (1997). “Carbon–carbon composites prepared by rapid densification process II: structure and texture characterizations,” *Carbon*, **35**, 1599–1611.
- Buckley, J. D. (1993). “Carbon/carbon materials and composites using CVD and CVI processing (an overview),” *Proceed. of 9th Inter. Conf. on Composite Mater.*, **3**, 675–682.
- Coffin, J. R. (1964). “Structure–properties relations for pyrolytic graphite,” *J. Am. Ceram. Soc.*, **47** (10), 473–478.
- David, P., Narcy, B., Ravel, Fr., and Houdayer, M. (1995). “Manufacturing of ceramic composites by rapid densification,” in *Proc. 2nd French–US Meeting for Technical Interchange on Carbon/Carbon Composites and Related High Temperature Materials*, La Jolla, CA, March 28–30, 1995.
- Diefendorf, R. J. (1960). “The deposition of pyrolytic graphite,” *J. Chim. Phys.*, **57**, 815–821.
- Diefendorf, R. J. (1970). “Deposition of pyrolytic carbons,” in *Reactivity of Solids*, J. W. Mitchell, R. C. De Vries, R. W. Roberts, and P. Cannon, eds, Wiley Publisher, 461–475.
- Doux, F. (1994). “La microscopie électronique en transmission au service des matériaux composites,” *Analisis Magazine*, **22**, 1, 31–34.
- Dupel, P., Pailler, R., Bourrat, X., and Naslain, R. (1994). “Pulse-chemical vapour deposition and infiltration of pyrocarbon in model pores with rectangular cross-sections: Part 2 – Study of the infiltration,” *J. Mater. Sci.*, **29**, 1056–1066.
- Dupel, P., Bourrat, X., and Pailler, R. (1995). “Structure of pyrocarbon infiltrated by pulse CVI,” *Carbon*, **33**(9), 1193–1204.
- Féron, O. (1998). “CVD/CVI du pyrocarbon – Analyse *in-situ* de la phase gazeuse – Etude cinétique et structurale,” Thèse No.1867, Université Bordeaux 1.
- Féron, O., Langlais, F., Naslain, R., and Thébault, J. (1999). “On kinetics and microstructural transitions in the CVD of pyrocarbon from propane,” *Carbon*, **37**, 1343–1353.
- Fillion, A. (2000). “Matériaux céramiques et traitements de surface,” Thèse No. 2168 Univ. Bordeaux 1 (France).
- Ford, L. H. and Bilsby, C. F. (1976). “Porosity related to structure for low temperature propylene pyrocarbons,” *J. of Nuclear Materials*, **60**, 79–88.

- Fujimoto, H., Tokumitsu, K., Mabuchi, A., Kasuh, T., and Shiraishi, M. (1994). "New structural parameters for carbon: comprehensive crystallization index and cavity index," *Carbon*, **32** (7), 1249–1252.
- Furuta, T., Sanada, Y., and Honda, H. (1969). "Core structure of phenol–formaldehyde resin carbons," *Carbon*, **7**, 510.
- Golecki, I., Morris, R. C., Naraimhan, D., and Clements, N. (1995). "Rapid densification of carbon-carbon by thermal-gradient chemical vapor infiltration," in Proc. of 19th Annual Conf. on Composites, Advanced Ceramics, Materials and Structures-A (Cocoa Beach), 315–322, Am. Ceram. Soc. ed.
- Goma, J. and Oberlin, A. (1985). "Microtexture and structure of high temperature massive pyrocarbons prepared on graphite substrates," *Carbon*, **23** (1), 85–90.
- Goma, J. and Oberlin, A. (1986). "Characterization of low temperature pyrocarbons obtained by densification of porous substrates," *Carbon*, **24** (2), 135–142.
- Granoff, B., Pierson, H. O., and Schuster, D. M. (1973). "The effect of chemical-vapor-deposition conditions of carbon on the properties of carbon–carbon composites," *Carbon*, **11**, 177–187.
- Grisdale, R. O. (1953). "The formation of black carbon," *J. of Appl. Phys.*, **24** (9), 1082–1091.
- Guentert, O. J. (1962). *J. Chem. Phys.*, **37**, 844–891.
- Hirai and Yajima (1967). "Structural Features of Pyrolytic Graphite," *J. of Mat. Science*, **2**, 18–27.
- Jacques, S., Guette, A., Langlais, F., and Bourrat, X. (1997). *J. of Mat. Science*, **32**, 2969–2975.
- Kaae, J. L., Gulden, T. D., and Liang, S. (1972). "Transmission electron microscopy of pyrolytic carbons deposited in a bed of fluidized particles," *Carbon*, **10**, 701–709.
- Kaae, J. L. (1975). "Microstructures of isotropic pyrolytic carbons," *Carbon*, **13**, 52–62.
- Kaae, J. L. (1985). "The mechanism of deposition of pyrolytic carbons," *Carbon*, **23**, 665–673.
- Kotlensky, W. V., Bauer, D. W., Warren, J. W., Smith, W. H., Gray, E., and Campbell, J. (1971). In Tenth Biennial Conference on Carbon, 80.
- Lamicq, P. J. (1984). "Propriétés et utilisation des composites carbone-carbone," *J. Chim. Phys.*, **81**, 11/12.
- Lavenac, J. (2000). "CVD/CVI de pyrocarbones laminaires à partir du propane. Processus chimiques homogènes et hétérogènes, nanostructure," Thèse Université Bordeaux 1, No. 0: 2274.
- Lavenac, J., Langlais, F., Féron, O., and Naslain, R. (2001). "Microstructure of the pyrocarbon matrix in carbon/carbon composites," *Composite Science and Technology*, **61**, 339–345.
- Le Carbone Lorraine (1975). Fiche technique , PSP, **11** (2), F, Ed. 4–75.
- Lieberman, M. L. and Pierson, H. O. (1974). "Effect of gas phase conditions on resultant matrix pyrocarbons," *Carbon*, **12**, 233–241.
- Loll, P., Delhaès, P., Pacault, A., and Pierre, A. (1977). "Diagramme d'existence et propriétés de composites carbone-carbone," *Carbon*, **15**, 383–390.
- Mar'yasin, I. L. and Tesner, P. A. (1961). *Doklady Akad. Nauk SSSR*, **140**, 5, 1121–24.
- Pierson, H. O. and Lieberman, M. L. (1975). "The chemical vapor deposition of carbon on carbon fibers," *Carbon*, **13**, 159–166.
- Oberlin, A. (1979). *Carbon*, **17**, 77.
- Pappis, J. and Blum, S. L. (1961). "Properties of Pyrolytic Graphite," *J. of Am. Ceram. Soc.*, **44**, 12, 592–597.
- Parker, W. G. and Wolfhard, H. G. (1950). *J. Chem. Soc.*, 2038.
- Pelissier, J. and Lombard, L. (1975). "Transmission electron microscopy of isotropic pyrocarbon deposited on spherical particles for high temperature reactor," *Carbon*, **13**, 205–210.
- Rovilain, D. (1999) "Procédé de densification rapide et caractérisation de composites carbone-carbone," Thèse Univ. Bordeaux 1, No. 0: 2067 (France).
- Rouzaud, J. N., and Oberlin, A. (1983). "Carbon films: structure and microtexture (optical and electron microscopy, Raman spectroscopy)," *Thin Solids Films* **105**, 75PR.
- Stokes, C. A. (1951). *J. Inst. Fuel*, **24**, 90.
- Sweitzer, C. N. and Heller, G. L. (1956). *Rubber World*, **134**, 855.

- Tessner, P. A. (1984). "Kinetics of pyrolytic carbon formation," in *Chemistry and Physics of Carbon*, P.A. Thrower ed., Marcel Dekker, New York, Vol. 19, 65–161.
- Thomas, A. (1962). *Combustible Flame*, **6**, 46.
- Tombrel, F. and Rappeneau, J. (1965). "Préparation et structure des pyrocarbones," ch. XXV in *Les Carbones*, A. Pacault ed., Dunod editeur Paris, 783–836.
- Warren, B. E. (1941). "X-ray diffraction in random layer lattices," *Phys. Rev.*, **59**, 693–699.